*Nano Research* 2018, 11(3): 1437–1446
https://doi.org/10.1007/s12274-017-1759-0
**Research Article**
ISSN 1998-0124
CN 11-5974/O4

# Hierarchical three-dimensional flower-like $Co_3O_4$ architectures with a mesocrystal structure as high capacity anode materials for long-lived lithium-ion batteries

Wenqiang Cao[1], Wenzhong Wang[1] (✉), Honglong Shi[1], Jun Wang[2], Maosheng Cao[3], Yujie Liang[1], and Min Zhu[1]

[1] *School of Science, Minzu University of China, Beijing 100081, China*
[2] *Faculty of Sciences, Ningbo University, Ningbo 315211, China*
[3] *School of Materials Science and Engineering, Beijing Institute of Technology, Beijing 100081, China*

**Received:** 20 April 2017
**Revised:** 8 July 2017
**Accepted:** 8 July 2017



**KEYWORDS**
$Co_3O_4$,
three-dimensional,
anode materials,
lithium-ion batteries

## ABSTRACT

In this work, we rationally design a high-capacity electrode based on three-dimensional (3D) hierarchical $Co_3O_4$ flower-like architectures with a mesocrystal nanostructure. The specific combination of the micro-sized 3D hierarchical architecture and the mesocrystal structure with a high porosity and single crystal-like nature can address the capacity fading and cycling stability as presented in many conversion electrodes for lithium-ion batteries. The hierarchical 3D flower-like $Co_3O_4$ architecture accommodates the volume change and mitigates mechanical stress during the lithiation–delithiation processes, and the mesocrystal structure provides extra lithium-ion storage and electron/ion transport paths. The achieved hierarchical 3D $Co_3O_4$ flower-like architectures with a mesocrystal nanostructure exhibit a high reversible capacity of 920 mA·h·g$^{-1}$ after 800 cycles at 1.12 C (1 C = 890 mA·h·g$^{-1}$), improved rate performance, and cycling stability. The finding in this work offers a new perspective for designing advanced and long-lived lithium-ion batteries.

## 1 Introduction

Currently, lithium-ion batteries are widely used as power sources for portable electronic devices and are generally regarded as one of the most promising power sources for electric vehicles [1, 2]. However, with the rapid development and popularization of charge-sustaining and plug-in hybrid electric vehicles as well as full electric vehicles, current commercial lithium-ion batteries that use a graphitic carbon anode are unable to satisfy the high power and energy storage capacity demands because of their relatively low energy density and specific capacity. Thus, exploring novel anode materials with higher capacities, power capabilities, and cycle performances is crucial to meet the demands of future energy storage devices, such as

Address correspondence to wzhwangmuc@163.com

next-generation electric vehicles [3–7].

A higher capacity, power capability, and cycle performance of the anode materials can be achieved for lithium-ion batteries by reducing the size of the electrode materials to the nanoscale regime or by fabricating hierarchical electrode materials with unique features, such as nano [8, 9], porous [7, 10], and mesocrystal [11–13] structures. Indeed, the electrochemical performances of lithium-ion batteries can be significantly improved by using electrodes fabricated with nanostructured materials, such as nanoparticles [14, 15], nanorods [16], nanowires [5, 17, 18], nanofibers [19], nanotubes [20, 21], nanosheets [22], and nanospheres [23], because nanostructured electrode materials can shorten the lithium-ion diffusion pathway, effectively relax the inner lattice stress, and reduce electrode exfoliation. However, the high surface area of nanoscale materials inherently forms a large quantity of solid-electrolyte interface (SEI) layers on the surface of the electrode with decomposition of the liquid electrolyte during cycling, while excessive SEI layers can consume electrolytes and lithium ions, leading to severe capacity fading [24]. One of the efficient strategies for solving this issue is to fabricate hierarchical electrode materials with nanostructured and/or mesocrystal structures [25–28].

In recent years, many articles have demonstrated that three-dimensional (3D) hierarchical architectures assembled by nanostructured building blocks can remarkably enhance the electrochemical performance of lithium-ion batteries [25–28]. The enhanced electrochemical performances are attributed to the following advantages: (1) 3D hierarchical electrode materials assembled by nanostructured building blocks can efficiently inhibit self-aggregation of electrode materials, maintaining large surface areas for efficient contact with the electrolyte. (2) 3D hierarchical electrode materials can effectively buffer the volume expansion and mitigate mechanical stress of the electrode during charge–discharge cycling, improving the structural stability of the electrode, and enhancing its capacity and cycle performance.

Beyond improving the electrochemical performances using hierarchical electrode materials with nanostructured building blocks, hierarchical electrode materials with mesocrystal structures can also significantly enhance the electrochemical performances of lithium-ion batteries [11–13]. Mesocrystals are oriented nanoparticle superstructures assembled by individual nanocrystals with common crystallographic orientations, and they generally possess intrinsic features, such as a large and rough surface area, high porosity, single-crystal-like structure, and micrometer size. These intrinsic features mean that mesocrystals are an intriguing and promising anode material for high-performance lithium-ion batteries. The large surface area of the mesocrystals ensures that they effectively contact with the electrolyte, enhancing the capacity. The high porosity of the mesocrystal provides extra space for lithium-ion storage and buffers the electrode volume expansion caused by lithium insertion/extraction, maintaining the structural stability of the electrode and improving the cycling performance and capacity. The single-crystal-like structure of the mesocrystals permits them to effectively eliminate grain boundaries at the interface with adjacent nanoparticles, providing much better charge transport and ultimately improving the electrochemical performances. The micrometer size of the mesocrystals prevents self-aggregation of electrode materials, buffers the volume expansion, and mitigates the mechanical stress of the electrode, improving the capacity and cycle performance.

In addition to designing and fabricating hierarchical electrode materials with unique features, another crucial strategy to enhance the electrochemical performances of lithium-ion batteries is to explore electrode materials with a high theoretical capacity and power capability. Recently, several 3d transition-metal oxides, such as $Co_3O_4$, NiO, $Fe_3O_4$ and CuO, have been proposed as promising alternative anode materials because they show remarkably higher theoretical capacities (~ 500–1,000 $mA{\cdot}h{\cdot}g^{-1}$) than those of commercialized graphite anode materials [29]. Among the 3d transition-metal oxides, $Co_3O_4$ is one of the most promising anode material for lithium-ion batteries because of its high theoretical specific capacity (~ 890 $mA{\cdot}h{\cdot}g^{-1}$) and high abundance [30–38]. The specific capacity of $Co_3O_4$ is more than two times higher than the value of commercialized graphite (~ 372 $mA{\cdot}h{\cdot}g^{-1}$); thus, $Co_3O_4$ anodes are anticipated to meet the demands of future energy storage devices. However, like other 3d

transition-metal oxides, the lithium storage of the $Co_3O_4$ anode is fulfilled by a reversible conversion reaction mechanism, which leads to volume expansion during the lithium-ion insertion/extraction process and results in capacity fading and a poor cyclability. Based on the advantages of 3D hierarchical architectures, mesocrystals, and nanostructures in lithium-ion batteries, the use of 3D hierarchical $Co_3O_4$ anode materials with a mesocrystal nanostructure is expected to be a promising and effective strategy to solve these issues.

Herein, we rationally design a high-capacity electrode based on 3D hierarchical $Co_3O_4$ flower-like architectures with a mesocrystal nanostructure. In this electrode, the nanostructure shortens the lithium-ion diffusion pathway and effectively relaxes the inner lattice stress; meanwhile, the mesocrystal structure provides extra space for lithium-ion storage, buffers the electrode volume expansion, and provides good electron conduction because of its high porosity and single-crystal-like nature. The 3D hierarchical architecture provides large surface areas, abundant active sites, and structural stability.

## 2 Experimental

### 2.1 Synthesis of the 3D hierarchical electrode material

The hierarchical 3D $Co_3O_4$ flowers with a mesocrystal nanostructure were synthesized using a facile two-step method. Specially, a surfactant-free hydrothermal method was employed to synthesize 3D $\alpha$-$Co(OH)_2$ flowers. $CoCl_2{\cdot}6H_2O$ (0.2 mmol), NaCl (1.0 mmol), hexamethylenetetramine (1.2 mmol), and absolute ethanol (2 mL) were dissolved in deionized water (180 mL) and stirred for 20 min. Subsequently, the solution was sealed in a 250-mL Teflon-lined autoclave and kept at 90 ℃ for 1 h. Then, the reaction solution was cooled to room temperature. The green precipitate was collected and washed several times with distilled water, centrifuged, and then dried at room temperature in air. Next, the as-prepared 3D $\alpha$-$Co(OH)_2$ flowers were annealed at 400 ℃ for 2 h and converted to hierarchical 3D $Co_3O_4$ flowers. After the heat-treated reaction was completed and the hierarchical 3D $Co_3O_4$ flowers were cooled to room temperature, and the black powders were collected for subsequent experiments.

### 2.2 Characterization

X-ray diffraction (XRD) was carried out using a Rigaku (Japan) D/max γA X-ray diffractometer (Cu K$\alpha$ radiation, $\lambda$ = 1.54178 Å) at room temperature. The morphology and structural features of the materials were investigated using a field-emission scanning electron microscope (Hitachi S-4800) with an energy-dispersive spectrometer and transmission electron microscope (JEOL-2100) operated at 200 keV. The specific surface area of the hierarchical 3D $Co_3O_4$ flowers was calculated using the Brunauer–Emmett–Teller (BET) and Barrett–Joyner–Halenda (BJH) methods by adsorption and desorption of nitrogen at −209 ℃ using a JW-BK122F instrument.

### 2.3 Cell preparation and electrochemical performance measurements

To prepare working electrodes, the powders of 70 wt.% $Co_3O_4$ active materials, 20 wt.% acetylene black, and 10 wt.% polyvinylidene difluoride binder were mixed completely and then coated onto a copper foil. The electrodes were dried at 80 ℃ in vacuum for 24 h. Electrochemical performances were evaluated using two-electrode CR 2032 coin-type cells with $Co_3O_4$ active materials as the working electrode, lithium foil as the counter electrode, and a Celgard 2400 membrane as the separator. The electrolyte was 1 M $LiPF_6$ dissolved in a 1:1:1 mixture (*v*/*v*) of ethylene carbonate, ethyl methyl carbonate, and dimethyl carbonate. The coin cells were assembled in an argon-filled glove box with oxygen and moisture contents below 1 ppm. Cyclic voltammetry (CV) tests were performed on a CHI 760c electrochemical workstation at room temperature. Galvanostatic charge–discharge measurements were carried out using a battery testing system (Land CT2001A) at room temperature.

## 3 Results and discussion

The 3D hierarchical $Co_3O_4$ flower-like architectures were synthesized by a two-step method. They were first synthesized by a surfactant-free low-temperature

chemical method. Second, the 3D hierarchical $Co_3O_4$ flower-like architectures were prepared by annealing the as-prepared 3D hierarchical $Co(OH)_2$ flowers. The morphologies of the 3D hierarchical $Co_3O_4$ flower-like architectures were evaluated using scanning electron microscopy (SEM). In Fig. 1(a), 3D hierarchical $Co_3O_4$ flower-like architectures with an average diameter of about 3.5 μm were achieved. The enlarged SEM images (Fig. 1(b)) demonstrate that the 3D hierarchical $Co_3O_4$ flower-like architectures are assembled by nanoplates with thicknesses of several tens of nanometers. Figures 1(c) and 1(d) show an SEM image of a single 3D $Co_3O_4$ flower-like architecture and its corresponding enlarged SEM image, respectively. Similarly, the architecture is assembled by nanoplates. The enlarged SEM image of Fig. 1(d) demonstrates that the nanoplates with large porosities consist of nanoparticles.

The structural features of the 3D hierarchical $Co_3O_4$ flower-like architectures were investigated by transmission electron microscopy (TEM), high-resolution TEM (HRTEM), and selected area electron diffraction (SAED). The TEM image (Fig. 2(a)) clearly demonstrates that the nanoplates are assembled to construct a 3D hierarchical $Co_3O_4$ flower-like architecture with many pores. The corresponding enlarged TEM image in Fig. 2(b) shows that the size distribution of these pores ranges from several to tens of nanometers. In Fig. 2(c), the HRTEM image displays obvious lattice

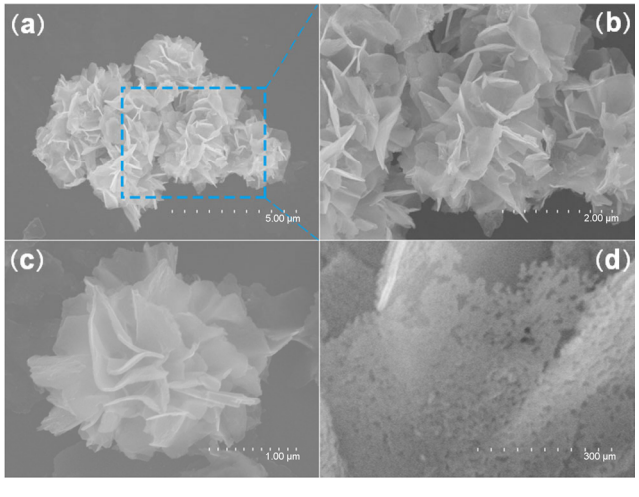


**Figure 1** (a) and (b) SEM and corresponding enlarged SEM images of the hierarchical 3D $Co_3O_4$ flower-like architectures. (c) SEM image of a single 3D $Co_3O_4$ flower-like architecture and (d) its corresponding enlarged SEM image.

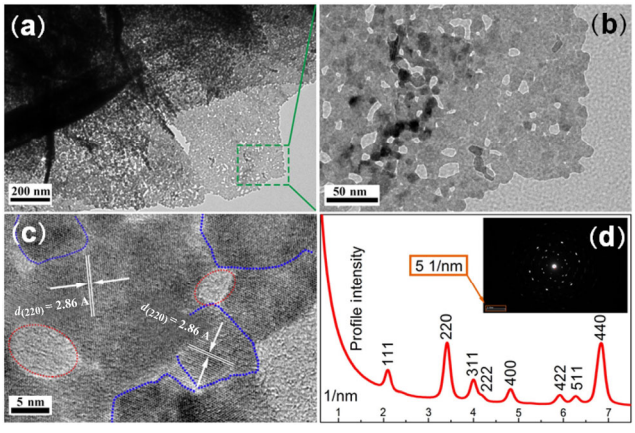


**Figure 2** (a) TEM and (b) enlarged TEM images of the materials. (c) HRTEM image and (d) the diffraction profile obtained from the SAED pattern (inset).

fringes with a 0.28-nm lattice spacing, which can be indexed to the (220) crystal planes of spinel crystallite $Co_3O_4$ along the [111] zone. The crystal phase of the 3D hierarchical $Co_3O_4$ architectures was investigated using the diffraction profile obtained from the SAED pattern (the inset in Fig. 2(d)). The diffraction profile in Fig. 2(d) shows characteristic diffraction peaks of the spinel $Co_3O_4$ crystallite (JCPDS 43-1003). The crystallization feature of the nanoplates is further evaluated by SAED. Spots with a hexagonal distribution of the SAED pattern (the inset in Fig. 2(d)) demonstrate that the nanoplates have single-crystal characteristics. Thus, the HRTEM and SAED results show that although the nanoplates that are assembled to construct 3D hierarchical $Co_3O_4$ architectures exhibit a remarkably porous structure, these nanoplates still present a single-crystal-like structure, which is consistent with the mesocrystal characteristic of crystals reported in the literature [39].

The composition and crystal phase of the prepared 3D hierarchical $Co_3O_4$ flower-like architectures were further studied using XRD. Figure 3 shows the XRD pattern of the obtained architectures. Nine diffraction peaks in the XRD pattern are easily indexed to the (220), (311), (222), (400), (422), (511), (440), (620), and (533) planes of spinel $Co_3O_4$ (JCPDS 43-1003). No diffraction peaks from hydroxides or other cobalt oxides are detected, showing that pure $Co_3O_4$ architectures are successfully synthesized. The XRD result for the composition and crystal phase studies

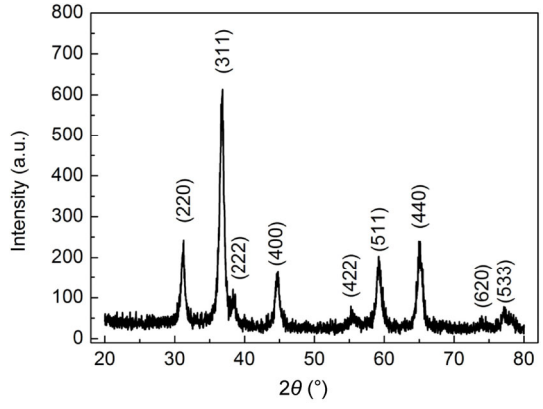


**Figure 3** The XRD patterns of the hierarchical 3D $Co_3O_4$ architectures.

of the $Co_3O_4$ flower-like architectures is in good agreement with the study of the diffraction profile obtained from the SAED pattern.

BET surface areas and BJH pore size distributions of the 3D hierarchical $Co_3O_4$ flower-like architectures with a mesocrystal nanostructure were evaluated from their nitrogen adsorption/desorption isotherms at 77 K. In Fig. 4, the nitrogen adsorption/desorption isotherms of the 3D hierarchical $Co_3O_4$ architectures exhibit a typical type-IV isotherm with a hysteresis loop, demonstrating the mesoporous nature of the 3D hierarchical $Co_3O_4$ flower-like architectures. The calculated specific BET surface area is 112.8 $m^2 \cdot g^{-1}$ with a total pore volume of 0.37 $cm^3 \cdot g^{-1}$. The inset in Fig. 4 shows the distribution curve for the pore size, showing an almost monomodal pore size distribution.

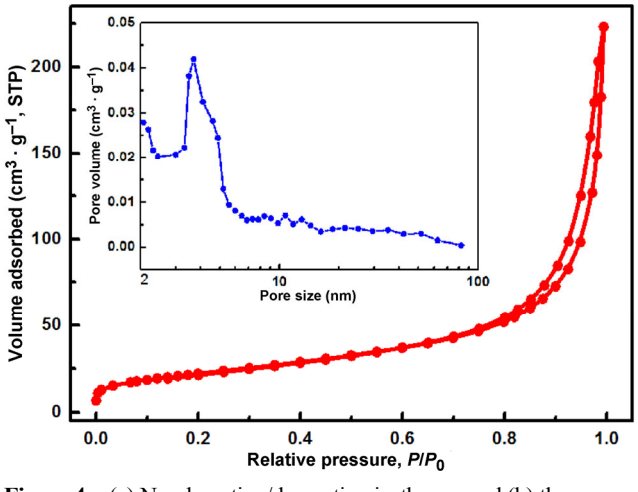


**Figure 4** (a) $N_2$ adsorption/desorption isotherms and (b) the corresponding pore size distribution of the as-achieved hierarchical 3D $Co_3O_4$ flower-like architectures.

The average pore size calculated by the BJH method is 3.8 nm.

The electrochemical properties of the electrodes made from our hierarchical 3D $Co_3O_4$ architectures with a mesocrystal nanostructure are first evaluated by CV measurements. In Fig. 5(a), the first cycle displays a strong peak at ~ 0.86 V, shoulder peak at 1.0 V, and weak peak at ~ 1.25 V in the discharge process. The shoulder cathodic peak can be ascribed to the initial reduction of $Co_3O_4$ to CoO with the generation of $Li_2O$ [12, 29–31]. This can be confirmed by the ~ 1.3 V plateau in the first discharge curve, as presented in Fig. 5(b). The cathodic peaks at ~ 0.86 and ~ 1.20 V are attributed to further reduction of CoO to metallic Co accompanied by the generation of $Li_2O$ and an SEI layer [12, 29–31]. This can also be confirmed by the ~ 1.0 V plateau in the first discharge curve (Fig. 5(b)). In the first charge process, a broad anodic peak centered at ~ 2.2 V is attributed to the reversible oxidation of Co to $Co_3O_4$ with the decomposition of $Li_2O$ [12, 29–31]. In the following second and third cycles, the cathodic peak shifts to ~ 1.15 V. The intensity of the cathodic peak decreases significantly, which is caused by the irreversible reaction accompanying the generation of the irreversible SEI layer in the first cycle [40]. In addition, the anodic peat at ~ 2.2 V shows a slight change, and the intensity of the anodic peaks and the integrated areas of the second and third cycles are

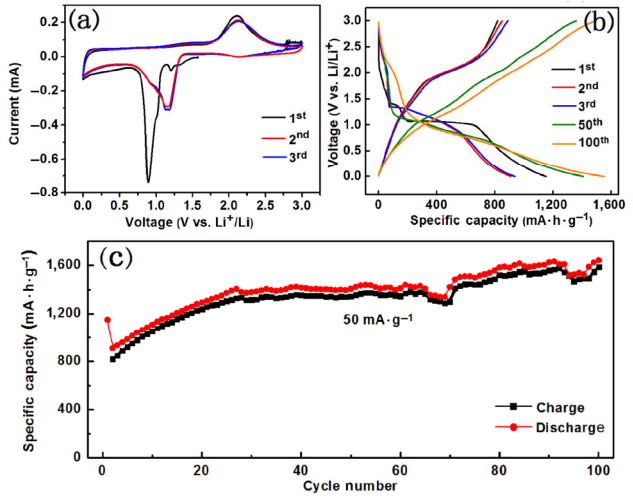


**Figure 5** (a) CVs of the 1st, 2nd, and 3rd cycles in the voltage range of 0.01–3.00 V. (b) Galvanostatic charge/discharge curves of the 1st, 2nd, 3rd, 50th, and 100th cycles at the same rate of 50 $mA \cdot g^{-1}$. (c) Cycle performance at a current density of 50 $mA \cdot g^{-1}$.

almost the same, indicating the good cycle stability and gradual improvement of the electrochemical reversibility for hierarchical 3D $Co_3O_4$ flower-like architectures after the first cycle. Thus, the total electrochemical reaction mechanism of $Co_3O_4$ can be given as follows

$$Co_3O_4 + 8Li^+ + 8e^- \leftrightarrow 4Li_2O + 3Co \quad (1)$$

The battery performances of the electrodes made from hierarchical 3D $Co_3O_4$ flower-like architectures with a mesocrystal nanostructure are further studied by galvanostatic charge–discharge cycling under a current density of 50 $mA \cdot g^{-1}$, as shown in Fig. 5(b). In the first discharge curve, a short voltage plateau at ~ 1.3 V and a long one at ~ 1.0 V correspond to the initial reduction of $Co_3O_4$ to CoO and then to metallic Co, respectively [12, 29–31], which is consistent with the above CV results. The electrode exhibits an initial discharge capacity of ~ 1,152 $mA \cdot h \cdot g^{-1}$ in the first cycle; then, the discharge capacity decreases to ~ 909 and 936 $mA \cdot h \cdot g^{-1}$ in the second and third cycles, respectively. Then, the discharge capacity gradually increases to 1,405 and 1,550 $mA \cdot h \cdot g^{-1}$ in the 50$^{th}$ and 100$^{th}$ cycles, respectively. Initially, the charge capacities during the second and third cycles also display gradual increases, as presented in the charge curves (Fig. 5(b)). The gradual capacity increase of our electrodes is partially attributed to the formation of a polymeric layer during electrolyte decomposition [33, 41, 42].

The superior battery performance of the electrodes built with our hierarchical 3D $Co_3O_4$ architectures is also confirmed based on their discharge–charge cycling performances. Figure 5(c) shows a discharge–charge profile and capacity retention over 100 cycles, which was evaluated at a current density of 50 $mA \cdot g^{-1}$ in the voltage range of 0.01 to 3.0 V at room temperature. It clearly demonstrates that the capacity increases gradually after the second cycle. Meanwhile, the electrode made using the hierarchical 3D $Co_3O_4$ architecture displays a superior capacity retention with a prolonged cycling and its Coulombic efficiency is maintained at ~95.6%. Remarkably, at the end of 100 cycles, the discharge capacity of the electrode reaches ~ 1,588 $mA \cdot h \cdot g^{-1}$, which is much higher than the value for mesoporous hexagonal $Co_3O_4$ [34]. The results clearly demonstrate the superior capacity and cycle life of our pure hierarchical 3D $Co_3O_4$ flower-like architectures. The excellent battery performance of the hierarchical 3D $Co_3O_4$ flower-like architecture is possibly attributed to its unique architecture with a hierarchical morphology, mesocrystal nanostructure (which can alleviate the mechanical stress caused by the volume change while prolonging charge–discharge cycling and provide extra space for lithium-ion storage), abundant active sites, and good electron conduction.

The rate capability of the electrodes further demonstrates the superior electrochemical properties of the hierarchical 3D $Co_3O_4$ flower-like architectures. Figure 6(a) shows a discharge–charge profile and capacity retention over 800 cycles at a high current rate of 1 $A \cdot g^{-1}$ (1.12 C, 1 C = 890 $mA \cdot h \cdot g^{-1}$, the theoretical capacity of $Co_3O_4$). The discharge–charge profile exhibits a drastic capacity fading, which decreases from 918 (at the second cycle) to 199 $mA \cdot h \cdot g^{-1}$ (at the 80$^{th}$ cycle), even though the hierarchical 3D $Co_3O_4$ flower-like architectures have a mesocrystal nanostructure. The tremendous capacity fading is possibly caused by formation of an unstable SEI layer, which is frequently observed in conversion-based 3d transition-metal oxide lithium-ion storage anode materials. However, the capacity of the electrode increases monotonically during the following cycles after fading to the lowest value at the 80$^{th}$ cycle. The increased capacity is attributed to continuous high-rate lithiation and

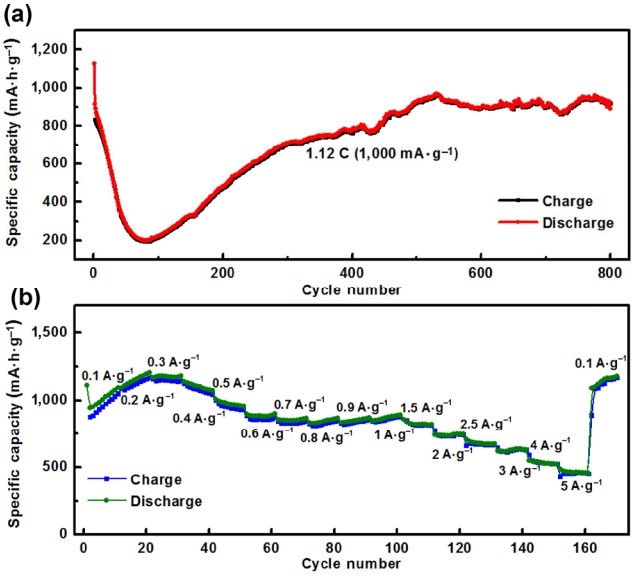


**Figure 6** (a) Long cycling performance at a rate of 1.12 C. (b) Rate performance.

the formation of a partially polymeric layer during electrolyte decomposition [3, 33, 41, 42]. At 1.12 C, the capacity reaches 930 mA·h·g$^{-1}$ during the 500$^{th}$ cycle, which is more than a 467% recovery from the lowest capacity value. Furthermore, a high capacity of 920 mA·h·g$^{-1}$ is achieved after 800 cycles at 1.12 C. The remarkably improved capacity represents more than a 240% improvement to the theoretical capacity of the commercialized graphite anode (~ 372 mA·h·g$^{-1}$).

The electrode built with our hierarchical 3D $Co_3O_4$ flower-like architectures with a mesocrystal nanostructure also displays a significantly enhanced rate capability. Figure 6(b) shows the rate capability of the hierarchical 3D $Co_3O_4$ flowers, which was evaluated at various rates from 0.1 A·g$^{-1}$ (0.11 C) to 5 A·g$^{-1}$ (5.62 C). The rate cycling performance demonstrates that the electrode can deliver a specific capacity of 1,007 mA·h·g$^{-1}$ at 0.1 A·g$^{-1}$ (0.11 C), 998 mA·h·g$^{-1}$ at 0.5 A·g$^{-1}$ (0.56 C), 871 mA·h·g$^{-1}$ at 1 A·g$^{-1}$ (1.12 C), 695 mA·h·g$^{-1}$ at 2.5 A·g$^{-1}$ (2.81 C), and 478 mA·h·g$^{-1}$ at 5 A·g$^{-1}$ (5.62 C). More importantly, the electrode can deliver a reversible capacity to its initial capacity of 1,144 mA·h·g$^{-1}$ at 0.1 A·g$^{-1}$ (0.11 C) after once successive sequence test. Furthermore, in the range of 0.1 A·g$^{-1}$ (0.11 C) to 5 A·g$^{-1}$ (5.62 C), the rate capability of the hierarchical 3D $Co_3O_4$ architectures is much better than that of the reported results [33]. The rate performance of the electrode constructed with the hierarchical 3D $Co_3O_4$ architectures is excellent. Thus, this finding reveals that the hierarchical 3D $Co_3O_4$ flower-like architectures exhibit a stable structural integrity and good charge transfer kinetics during the lithium-ion insertion/de-insertion. In addition, the hierarchical 3D $Co_3O_4$ flower-like architectures with a mesocrystal nanostructure show a good electrochemical performance as promising metal oxide candidates for anode materials.

The reaction kinetics of the hierarchical 3D $Co_3O_4$ flower-like architectures was investigated using electrochemical impedance spectroscopy in a frequency range from 100 kHz to 0.1 Hz, as shown in Fig. 7. The Nyquist plot of both cycles exhibits depressed semicircles in the high and medium frequency ranges followed by inclined lines in the low frequency range. The inset in Fig. 7 presents the equivalent electrical circuit, where $R_\Omega$ is the solution resistance, $R_{ct}$ is the charge-transfer resistance at the interface between the electrolyte and electrode, $C_s$ is the double layer capacitance, and $Z_\omega$ is the Warburg impedance. $R_{ct}$ is associated with the diameter of the semicircle. The values of $R_{ct}$ for the 20$^{th}$ and 1$^{st}$ cycles are 82 and 253 Ω, respectively. The lower $R_{ct}$ at the 20$^{th}$ cycle means that an enhanced ion transfer property is achieved. Furthermore, the Nyquist curve of the 20$^{th}$ cycle exhibits a more vertical Warburg slope than that of the 1$^{st}$ cycle, revealing an excellent ion conductivity for the hierarchical 3D $Co_3O_4$ flower-like electrode.

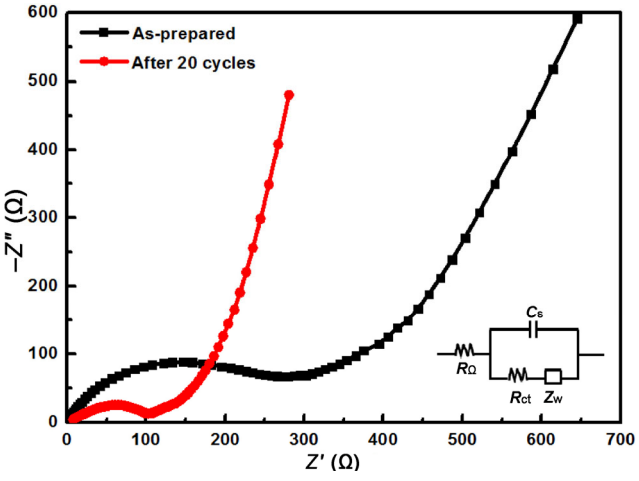


**Figure 7** The impedance spectra of the hierarchical 3D $Co_3O_4$ flower-like electrode during the 1$^{st}$ cycle and after 20 cycles.

The structural stability of the hierarchical 3D $Co_3O_4$ flower-like architectures was confirmed by SEM studies after 800 cycles at 1.12 C. Figure 8 shows SEM images of the samples obtained by disassembling the coin cell. Low- and high-magnification SEM images demonstrate that the 3D flower-like architecture is maintained even after long and intensive battery operation. We attribute the stable performance during lithium-ion insertion and extraction of the hierarchical 3D $Co_3O_4$ flower-like architecture to its novel and robust structure.

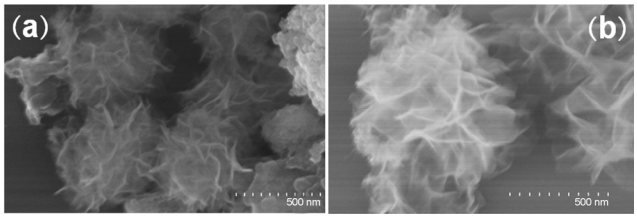


**Figure 8** (a) and (b) SEM images of $Co_3O_4$ architectures after 800 cycles at 1.12 C.

These results demonstrate that the designed electrode based on hierarchical 3D flower-like architectures with a mesocrystal nanostructure can achieve a stable electrochemical performance for long-lived lithium-ion batteries in metal oxide anodes. Such a design possesses multiple advantages: First, the micro-size hierarchical 3D $Co_3O_4$ flower-like architecture can offer large surface areas for efficient contact with the electrolyte, which effectively buffers the volume expansion and mitigates mechanical stress on the electrode during charge–discharge cycling, leading to a remarkable enhancement for the capacity of lithium-ion batteries, structural stability of the electrode, and cycle performance. These conclusions can be evidently confirmed by the high BET surface areas and long-lived cycling performances (Fig. 6(a)) of the hierarchical 3D $Co_3O_4$ flower-like architectures. Second, the mesocrystal structure featuring a high porosity and single-crystal-like nature, as shown in Fig. 2, can provide extra space for lithium-ion storage, buffer the electrode volume expansion, and provide good electron conduction, ultimately improving the electrochemical performances of the hierarchical 3D $Co_3O_4$ flower-like architectures (as confirmed in Figs. 5 and 6). In summary, this hierarchical 3D flower-like architecture with a mesocrystal nanostructure can maintain excellent structural properties and exhibit a better electrochemical performance than $Co_3O_4$ nanostructures, as given in Table 1.

Since nanostructured transition-metal oxides were first exploited as anode materials for lithium-ion batteries [29], many conversion materials have been developed as anode materials for lithium-ion batteries. However, as for alloy anode materials, conversion anode materials often suffer from severe capacity fading and poor cyclability caused by degradation of the material structure and large volume expansion during the lithium-ion insertion/extraction process. Here, we design an electrode from a hierarchical architecture of 3D flowers with a mesocrystal nanostructure to address these issues. The structural characteristics and electrochemical performance investigations clearly demonstrate that the achieved hierarchical architecture of 3D $Co_3O_4$ flowers with a mesocrystal nanostructure combines desirable mechanical properties and the required electrochemical performance for a high capacity rate and stable cycling for long-lived lithium-ion batteries. The micro-sized hierarchical 3D flower-like $Co_3O_4$ architecture buffers the large volume change and mitigates mechanical stress. The mesocrystal structure provides extra lithium-ion storage and buffers the large volume change of the electrode. The designed electrode shows promising practical applications in advanced and long-lived lithium-ion batteries with high capacities.

## 4 Conclusions

We developed lithium-ion battery electrodes from a hierarchical 3D metal oxide flower-like architecture with a mesocrystal nanostructure. The specific combination of hierarchical architectures with the micro

**Table 1** The structure and electrochemical Li cycling data of $Co_3O_4$ structures

| Morophology | Current rat ($mA \cdot g^{-1}$) | Cycling number | Reversible capacity ($mA \cdot h \cdot g^{-1}$) | Ref. |
|---|---|---|---|---|
| Plate-like mesocrystals | 1 C | 30 | 618 | [12] |
| Mesocrystal nanoplatelets | 1 C | 100 | 995 | [13] |
| Nanosheet-assembled hollow spheres | 0.2 C | 50 | 866 | [26] |
| Porous hollow dodecahedra | 100 | 100 | 780 | [30] |
| Porous hollow nanospheres | 100 | 100 | 820 | [31] |
| Nanosheet-assembled hierarchical nanostructures | 0.2 C | 80 | 888 | [33] |
| Mesoporous nanoplates | 1 C | 100 | 689 | [34] |
| Porous nanosheets | 500 | 240 | 1,380 | [35] |
| Nanocages | 500 | 100 | 810 | [36] |
| 3D hierarchical flower-like architectures | 1.12 C | 800 | 920 | This work |

size and mesocrystal structure provides a high porosity and single-crystal-like nature, which can address cycling stability challenges that are present in many conversion battery electrodes. The achieved hierarchical 3D $Co_3O_4$ flower-like architecture with a mesocrystal nanostructure displays a high reversible capacity (i.e., higher than the theoretical value [30–38]), improved rate performance, and cycling stability. This work offers a new strategy for designing advanced and long-lived lithium-ion batteries.

## Acknowledgements

This work was supported by the National Natural Science Foundation of China (Nos. 11374377, 61575225, 11404414, 11074312 and 11474174), and the Undergraduate Research Training Program of Minzu University of China (Nos. GCCX2016110009 and GCCX2016110010).

## References

[1] Tarascon, J. M.; Armand, M. Issues and challenges facing rechargeable lithium batteries. *Nature* **2001**, *414*, 359–367.

[2] Goodenough, J. B.; Kim, Y. Challenges for rechargeable Li batteries. *Chem. Mater.* **2010**, *22*, 587–603.

[3] Sun, H. T.; Xin, G. Q.; Hu, T.; Yu, M. P.; Shao, D. L.; Sun, X.; Lian, J. High-rate lithiation-induced reactivation of mesoporous hollow spheres for long-lived lithium-ion batteries. *Nat. Commun.* **2014**, *5*, 4526.

[4] Chan, C. K.; Peng, H. L.; Liu, G.; McIlwrath, K.; Zhang, X. F.; Huggins, R. A.; Cui, Y. High-performance lithium battery anodes using silicon nanowires. *Nat. Nanotechnol.* **2008**, *3*, 31–35.

[5] Li, Y. G.; Tan, B.; Wu, Y. Y. Mesoporous $Co_3O_4$ nanowire arrays for lithium ion batteries with high capacity and rate capability. *Nano Lett.* **2008**, *8*, 265–270.

[6] Sathiya, M.; Rousse, G.; Ramesha, K.; Laisa, C. P.; Vezin, H.; Sougrati, M. T.; Doublet, M. L.; Foix, D.; Gonbeau, D.; Walker, W. et al. Reversible anionic redox chemistry in high-capacity layered-oxide electrodes. *Nat. Mater.* **2013**, *12*, 827–835.

[7] Guo, B. K.; Wang, X. Q.; Fulvio, P. F.; Chi, M. F.; Mahurin, S. M.; Sun, X. G.; Dai, S. Soft-templated mesoporous carbon-carbon nanotube composites for high performance lithium-ion batteries. *Adv. Mater.* **2011**, *23*, 4661–4666.

[8] Aricò, A. S.; Bruce, P.; Scrosati, B.; Tarascon, J. M.; van Schalkwijk, W. Nanostructured materials for advanced energy conversion and storage devices. *Nat. Mater.* **2005**, *4*, 366–377.

[9] Wu, H. B.; Chen, J. S.; Hng, H. H.; Lou, X. W. Nanostructured metal oxide-based materials as advanced anodes for lithium-ion batteries. *Nanoscale* **2012**, *4*, 2526–2542.

[10] Zhou, Y.; Candelaria, S. L.; Liu, Q.; Uchaker, E.; Cao, G. Z. Porous carbon with high capacitance and graphitization through controlled addition and removal of sulfur-containing compounds. *Nano Energy* **2015**, *12*, 567–577.

[11] Uchake, E.; Cao, G. Z. Mesocrystals as electrode materials for lithium-ion batteries. *Nano Today* **2014**, *9*, 499–524.

[12] Wang, F.; Lu, C. C.; Qin, Y. F.; Liang, C. C.; Zhao, M. S.; Yang, S. C.; Sun, Z. B.; Song, X. P. Solid state coalescence growth and electrochemical performance of plate-like $Co_3O_4$ mesocrystals as anode materials for lithium-ion batteries. *J. Power Sources* **2013**, *235*, 67–73.

[13] Su, D. W.; Dou, S. X.; Wang, G. X. Mesocrystal $Co_3O_4$ nanoplatelets as high capacity anode materials for Li-ion batteries. *Nano Res.* **2014**, *7*, 794–803.

[14] Wu, Z. S.; Ren, W. C.; Wen, L.; Gao, L. B.; Zhao, J. P.; Chen, Z. P.; Zhou, G. M.; Li, F.; Cheng, H. M. Graphene anchored with $Co_3O_4$ nanoparticles as anode of lithium ion batteries with enhanced reversible capacity and cyclic performance. *ACS Nano* **2010**, *4*, 3187–3194.

[15] Hu, T.; Xin, G. Q.; Sun, H. T.; Sun, X.; Yu, M. P.; Liu, C. S.; Lian, J. Electrospray deposition of a $Co_3O_4$ nanoparticles-graphene composite for a binder-free lithium ion battery electrode. *RSC Adv.* **2014**, *4*, 1521–1525.

[16] Chen, S.; Wang, M.; Ye, J. F.; Cai, J. G.; Ma, Y. R.; Zhou, H. H.; Qi, L. M. Kinetics-controlled growth of aligned mesocrystalline $SnO_2$ nanorod arrays for lithium-ion batteries with superior rate performance. *Nano Res.* **2013**, *6*, 243–252.

[17] Nam, K. T.; Kim, D. W.; Yoo, P. J.; Chiang, C. Y.; Meethong, N.; Hammond, P. T.; Chiang, Y. M.; Belcher, A. M. Virus-enabled synthesis and assembly of nanowires for lithium ion battery electrodes. *Science* **2006**, *312*, 885–888.

[18] Tan, G. Q.; Wu, F.; Yuan, Y. F.; Chen, R. J.; Zhao, T.; Yao, Y.; Qian, J.; Liu, J. R.; Ye, Y. S.; Shahbazian-Yassar, R. et al. Freestanding three-dimensional core–shell nanoarrays for lithium-ion battery anodes. *Nat. Commun.* **2016**, *7*, 11774.

[19] Shen, Z.; Hu, Y.; Chen, Y. L.; Zhang, X. W.; Wang, K. H.; Chen, R. Z. Tin nanoparticle-loaded porous carbon nanofiber composite anodes for high current lithium-ion batteries. *J. Power Sources* **2015**, *278*, 660–667.

[20] Meng, J. S.; Niu, C. J.; Liu, X.; Liu, Z.; Chen, H. L.; Wang, X. P.; Li, J. T.; Chen, W.; Guo, X. F.; Mai, L. Q. Interface-modulated approach toward multilevel metal oxide nanotubes for lithium-ion batteries and oxygen reduction reaction.

*Nano Res*. **2016**, *9*, 2445–2457.

[21] Lou, X. W.; Deng, D.; Lee, J. Y.; Feng, J.; Archer, L. A. Self-supported formation of needlelike $Co_3O_4$ nanotubes and their application as lithium-ion battery electrodes. *Adv*. *Mater*. **2008**, *20*, 258–262.

[22] Wang, S. W.; Wang, L. J.; Zhang, K.; Zhu, Z. Q.; Tao, Z. L.; Chen, J. Organic $Li_4C_8H_2O_6$ nanosheets for lithium-ion batteries. *Nano Lett*. **2013**, *13*, 4404–4409.

[23] Wang, C.; Wang, F. X.; Zhao, Y. J.; Li, Y. H.; Yue, Q.; Liu, Y. P.; Liu, Y.; Elzatahry, A. A.; Al-Enizi, A.; Wu, Y. P. et al. Hollow $TiO_{2-X}$ porous microspheres composed of well-crystalline nanocrystals for high-performance lithium-ion batteries. *Nano Res*. **2016**, *9*, 165–173.

[24] Aurbach, D. Electrode-solution interactions in Li-ion batteries: A short summary and new insights. *J. Power Sources* **2003**, *119–121*, 497–503.

[25] Koo, B.; Xiong, H.; Slater, M. D.; Prakapenka, V. B.; Balasubramanian, M.; Podsiadlo, P.; Johnson, C. S.; Rajh, T.; Shevchenko, E. V. Hollow iron oxide nanoparticles for application in lithium ion batteries. *Nano Lett*. **2012**, *12*, 2429–2435.

[26] Wang, X.; Wu, X. L.; Guo, Y. G.; Zhong, Y. T.; Cao, X. Q.; Ma, Y.; Yao, J. N. Synthesis and lithium storage properties of $Co_3O_4$ nanosheet-assembled multishelled hollow spheres. *Adv*. *Funct*. *Mater*. **2010**, *20*, 1680–1686.

[27] Zhao, D. D.; Wang, L.; Yu, P.; Zhao, L.; Tian, C. G.; Zhou, W.; Zhang, L.; Fu, H. G. From graphite to porous graphene-like nanosheets for high rate lithium-ion batteries. *Nano Res*. **2015**, *8*, 2998–3010.

[28] Zhu, J. X.; Yin, Z. Y.; Yang, D.; Sun, T.; Yu, H.; Hoster, H. E.; Hng, H. H.; Zhang, H.; Yan, Q. Y. Hierarchical hollow spheres composed of ultrathin $Fe_2O_3$ nanosheets for lithium storage and photocatalytic water oxidation. *Energ*. *Environ*. *Sci*. **2013**, *6*, 987–993.

[29] Poizot, P.; Laruelle, S.; Grugeon, S.; Dupont, L.; Tarascon, J. M. Nano-sized transition-metal oxides as negative-electrode materials for lithium-ion batteries. *Nature* **2000**, *407*, 496–499.

[30] Wu, R. B.; Qian, X. K.; Rui, X. H.; Liu, H.; Yadian, B.; Zhou, K.; Wei, J.; Yan, Q. Y.; Feng, X. Q.; Long, Y. et al. Zeolitic imidazolate framework 67-derived high symmetric porous $Co_3O_4$ hollow dodecahedra with highly enhanced lithium storage capability. *Small* **2014**, *10*, 1932–1938.

[31] Ge, D. H.; Geng, H. B.; Wang, J. Q.; Zheng, J. W.; Pan, Y.; Cao, X. Q.; Gu, H. W. Porous nano-structured $Co_3O_4$ anode materials generated from coordination-driven self-assembled aggregates for advanced lithium ion batteries. *Nanoscale* **2014**, *6*, 9689–9694.

[32] Chen, M. H.; Xia, X. H.; Yin, J. H.; Chen, Q. G. Construction of $Co_3O_4$ nanotubes as high-performance anode material for lithium ion batteries. *Electrochim*. *Acta* **2015**, *160*, 15–21.

[33] Mujtaba, J.; Sun, H. Y.; Huang, G. Y.; Mølhave, K.; Liu, Y. G.; Zhao, Y. Y.; Wang, X.; Xu, S. M.; Zhu, J. Nanoparticle decorated ultrathin porous nanosheets as hierarchical $Co_3O_4$ nanostructures for lithium ion battery anode materials. *Sci*. *Rep*. **2016**, *6*, 20592.

[34] Su, D. W.; Xie, X. Q.; Munroe, P.; Dou, S. X.; Wang, G. X. Mesoporous hexagonal $Co_3O_4$ for high performance lithium ion batteries. *Sci*. *Rep*. **2014**, *4*, 6519.

[35] Li, Z. P.; Yu, X. Y.; Paik, U. Facile preparation of porous $Co_3O_4$ nanosheets for high-performance lithium ion batteries and oxygen evolution reaction. *J. Power Sources* **2016**, *310*, 41–46.

[36] Wang, Y.; Wang, B. F.; Xiao, F.; Huang, Z. G.; Wang, Y. J.; Richardson, C.; Chen, Z. X.; Jiao, L. F.; Yuan, H. T. Facile synthesis of nanocage $Co_3O_4$ for advanced lithium-ion batteries. *J. Power Sources* **2015**, *298*, 203–208.

[37] Wang, X. L.; Zhang, J. M.; Kong, X.; Huang, X.; Shi, B. Increasing rigidness of carbon coating for improvement of electrochemical performances of $Co_3O_4$ in Li-ion batteries. *Carbon* **2016**, *104*, 1–9.

[38] Tan, Y. L.; Gao, Q. M.; Li, Z. Y.; Tian, W. Q.; Qian, W. W.; Yang, C. X.; Zhang, H. Unique 1D $Co_3O_4$ crystallized nanofibers with (220) oriented facets as high-performance lithium ion battery anode material. *Sci*. *Rep*. **2016**, *6*, 26460.

[39] Wang, T. X.; Cölfen, H.; Antonietti, M. Nonclassical crystallization: Mesocrystals and morphology change of $CaCO_3$ crystals in the presence of a polyelectrolyte additive. *J*. *Am*. *Chem*. *Soc*. **2005**, *127*, 3246–3247.

[40] Hou, C.; Lang, X. Y.; Han, G. F.; Li, Y. Q.; Zhao, L.; Wen, Z.; Zhu, Y. F.; Zhao, M.; Li, J. C.; Lian, J. S. et al. Integrated solid/nanoporous copper/oxide hybrid bulk electrodes for high-performance lithium-ion batteries. *Sci*. *Rep*. **2013**, *3*, 2878.

[41] Huang, G. Y.; Xu, S. M.; Lu, S. S.; Li, L. Y.; Sun, H. Y. Micro-/nanostructured $Co_3O_4$ anode with enhanced rate capability for lithium-ion batteries. *ACS Appl*. *Mater*. *Interfaces* **2014**, *6*, 7236–7243.

[42] Lou, X. W.; Deng, D.; Lee, J. Y.; Archer, L. A. Thermal formation of mesoporous single-crystal $Co_3O_4$ nano-needles and their lithium storage properties. *J*. *Mater*. *Chem*. **2008**, *18*, 4397–4401.